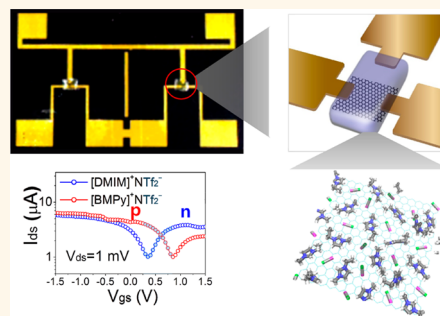


Modulation of the Dirac Point Voltage of Graphene by Ion-Gel Dielectrics and Its Application to Soft Electronic Devices

Un Jeong Kim,^{†,○} Tae Geun Kim,^{*,#} Youngseon Shim,[§] Yeonsang Park,[†] Chang-Won Lee,[†] Tae-Ho Kim,[†] Hyo Sug Lee,[§] Dae-Young Chung,^{||} Jineun Kihm,[†] Young-Geun Roh,[†] Jaesoong Lee,[†] Hyungbin Son,[⊥] Sangsig Kim,[#] Jaehyun Hur,^{*,∇} and Sung Woo Hwang^{*,†,‡}

[†]Nano Electronics Laboratory, Samsung Advanced Institute of Technology, Suwon, Gyeonggi-do 443-803, South Korea, [‡]Research Center for Time-Domain Nano-functional Devices, Samsung Advanced Institute of Technology, Suwon, Gyeonggi 443-803, South Korea, [§]CAE Group, Platform Technology Laboratory, Samsung Advanced Institute of Technology, Suwon, Gyeonggi-do 443-803, South Korea, ^{||}Organic Material Lab, Samsung Advanced Institute of Technology, Suwon, Gyeonggi-do 443-803, South Korea, [⊥]School of Integrative Engineering, Chung-Ang University, Seoul 156-756, South Korea, [#]Department of Electrical Engineering, Korea University, Anam-dong, Seongbuk-gu, Seoul 136-713, South Korea, and [∇]Department of Chemical and Biological Engineering, Gachon University, Seongnam, Gyeonggi-do 461-701, South Korea. [○]U.J.K. and T.G.K. contributed equally to this work.

ABSTRACT We investigated systematic modulation of the Dirac point voltage of graphene transistors by changing the type of ionic liquid used as a main gate dielectric component. Ion gels were formed from ionic liquids and a non-triblock-copolymer-based binder involving UV irradiation. With a fixed cation (anion), the Dirac point voltage shifted to a higher voltage as the size of anion (cation) increased. Mechanisms for modulation of the Dirac point voltage of graphene transistors by designing ionic liquids were fully understood using molecular dynamics simulations, which excellently matched our experimental results. It was found that the ion sizes and molecular structures play an essential role in the modulation of the Dirac point voltage of the graphene. Through control of the position of their Dirac point voltages on the basis of our findings, complementary metal–oxide–semiconductor (CMOS)-like graphene-based inverters using two different ionic liquids worked perfectly even at a very low source voltage ($V_{DD} = 1$ mV), which was not possible for previous works. These results can be broadly applied in the development of low-power-consumption, flexible/stretchable, CMOS-like graphene-based electronic devices in the future.



KEYWORDS: ion-gel dielectric · graphene transistor · flexible devices

Graphene is a two-dimensional (2d) carbon material that has unique physical properties and has attracted tremendous attention from scientists and engineers worldwide for over a decade. Its high electron mobility and mechanical flexibility make it attractive for electronic device applications such as radio-frequency transistors,^{1–3} and field-effect transistors (FETs).^{4–7} To adapt graphene for use in flexible and stretchable electronic devices,^{8–11} the incorporation of soft dielectrics, which determine the operating voltage range, on/off ratio, and mobility, is one of the key obstacles.^{12–16}

An ion gel is a composite of an ionic liquid and a polymeric binder. Ion gels were originally developed by Frisbie and co-workers, who mixed 1-ethyl-3-methylimidazolium bis(trifluoromethylsulfonyl)imide

([EMIM]⁺NTf₂[−]) with a triblock copolymer, poly(styrene-*b*-methyl methacrylate-*b*-styrene) (PS-PMMA-PS) or poly(styrene-*b*-ethylene oxide-*b*-styrene) (PS-PEO-PS), to form a physically cross-linked gel.^{17,18}

Many researchers have simply adopted these materials as the gate dielectrics in FETs because of their high capacitance ($\sim 10 \mu\text{F}/\text{cm}^2$), low operation voltage (< 2 V), mechanical flexibility, transparency, and facile processing.^{18,19} Moreover, the use of these materials has recently been extended to electrochemical energy storage applications, since as solid-state electrolytes they possess low volatility, good chemical stability, and wide electrochemical windows (EWs).^{20,21} Recognizing the importance of ion-gel systems as candidate gate dielectric materials, recent work has reported the use of ionic liquid components other

* Address correspondence to jhhur@gachon.ac.kr, swnano.hwang@samsung.com.

Received for review October 16, 2014 and accepted January 5, 2015.

Published online January 05, 2015
10.1021/nn505925u

© 2015 American Chemical Society

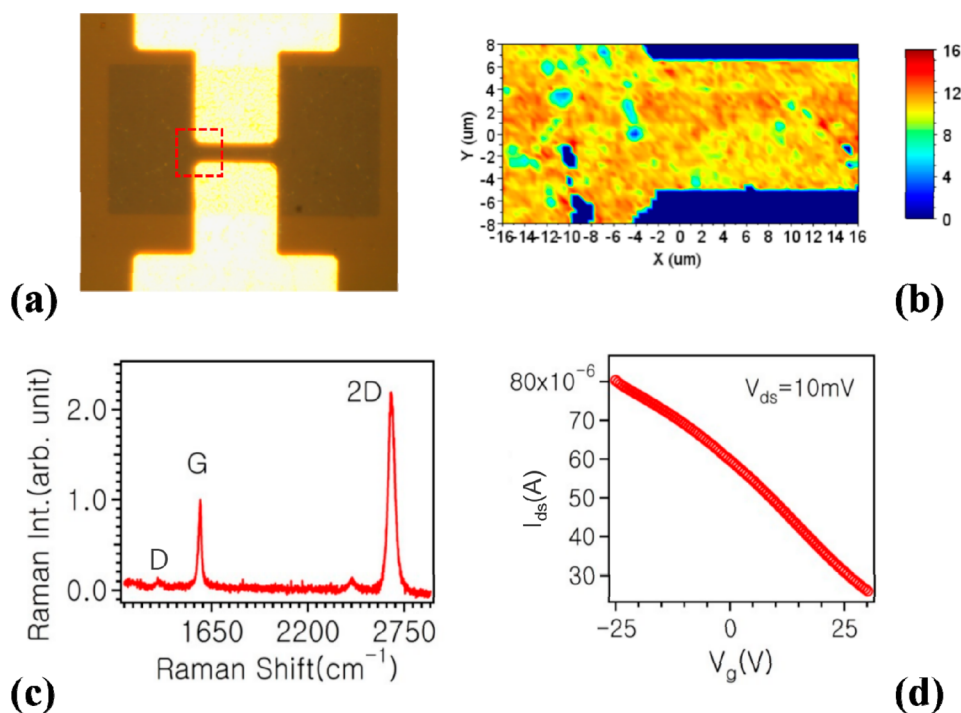


Figure 1. (a) Optical micrograph of a CVD-grown graphene transistor. (b) 2d Raman map showing the ratio of the intensity of the 2D band to that of the G band in the dotted rectangular area in (a). (c) Representative Raman spectrum of one spot on the graphene device measured under 532 nm laser excitation. (d) Dependence of the drain current (I_{ds}) on the gate voltage (V_g) at a drain voltage (V_{ds}) of 10 mV.

than $[\text{EMIM}]^+\text{NTf}_2^-$.^{22,23} In different approaches, other works introduced a new UV-cross-linkable binder, a combination of poly(ethylene glycol) diacrylate and a photoinitiator, for poly(3-hexylthiophene) (P3HT)-based FET systems to replace the polymeric binder; this advance enabled the photopatterning of ion gels on graphene or other organic nanomaterials.^{24–26}

However, to the best of our knowledge, there have been no serious efforts to understand the mechanism controlling the transport properties of graphene transistors that explicitly involve the molecular features of the ions in the ionic liquid used as a gate dielectric. In this work, we carried out a systematic and extensive study of graphene FET systems by incorporating nine different ion gels containing a non-triblock-copolymer-based binder. The primary purpose of this work was to understand how the physics at the ionic liquid–graphene interface influences the device performance and to leverage the results in the development of graphene-based complementary metal–oxide–semiconductor (CMOS)-like electronic devices. In addition, we fabricated an inverter made of graphene transistors with two different types of ion gel that can be operated at a very low supply voltage ($V_{DD} = 1$ mV) using our approach. Molecular dynamics (MD) simulations of the interfaces between the graphene and ionic liquids were performed to further understand our experimental observations. These findings on mechanisms for modulating the Dirac point voltage

of graphene by ionic liquids can be applied in the design of ionic liquids for use in graphene transistors. This work can be extended to the development of low-power flexible/stretchable integrated circuits such as ring oscillators and logic gates (*e.g.*, NAND and NOR gates).

RESULTS AND DISCUSSION

Figure 1 shows the results of our characterization of back-gate graphene transistors formed on Si/SiO₂ (100 nm). An optical micrograph of a graphene transistor in the back-gate configuration is shown in Figure 1a. A 2d Raman map indicating the ratio of the intensity of the 2D band to that of G band collected in the dotted rectangular area in Figure 1a is shown in Figure 1b. Using this map, we confirmed that the graphene was transferred successfully, though small holes in the graphene were sporadically observed. Very large values of the 2D/G intensity ratio indicated that our chemical vapor deposition (CVD)-grown graphene was a monolayer.²⁷ Figure 1c shows the characteristic Raman spectrum of a representative spot in the graphene, which indicates that the CVD-grown graphene was highly crystalline, as seen from the D/G intensity ratio. The electrical properties of the CVD-grown, back-gate-configuration graphene transistor were studied prior to the addition of the ion gel to the device as a gate dielectric. Figure 1d shows the gate voltage (V_g) dependence of the drain current (I_{ds}) at a drain potential (V_{ds}) of 10 mV. As is well-known, graphene

transistors exhibit poor on/off ratios (<10). The field-effect mobility (μ) was obtained using

$$\mu = \Delta\sigma / (C_g \Delta V_g) = \left(\frac{\Delta I_{ds}}{V_{ds}} \frac{L}{W} \right) / (C_g \Delta V_g) \quad (1)$$

where W ($=40 \mu\text{m}$) is the channel width, L ($=10 \mu\text{m}$) is the channel length, and C_g ($=33 \text{ nF/cm}^2$) is the capacitance of the gate dielectric. As a result of oxygen adsorption, the transfer curves for back-gated graphene transistors under ambient conditions are p-type, and no Dirac point voltage was observed in this V_g range even though graphene is intrinsically ambipolar.²⁷

The deposition of the ion-gel dielectric is described schematically in Figure 2a. To study the influence of the ionic liquid on the transport properties of the graphene transistor, nine different ionic liquids were selected systematically; they are listed in Table 1 along with their molecular structures, molecular weights, and EWs (some of this information was obtained from ref 28). The ionic liquids were selected primarily by varying the anion with a fixed cation component of $[\text{EMIM}]^+$ (see entries 1–5 in Table 1). The anions are listed in the order of molecular weight, with the lowest at the top. For experiments where the anion was fixed as NTf_2^- , the associated various cations are listed in entries 6–9 in Table 1. Figure 2b shows the transfer curves (I_{ds} vs V_{gs}) measured at $V_{ds} = 1 \text{ mV}$ for graphene transistors with ion-gel dielectrics with $[\text{EMIM}]^+$ as the cation and five different anions (the “[EMIM]⁺ series”). In all cases, the ion-gel-gated graphene transistors exhibited ambipolar characteristics.

Three important aspects of the device function were revealed by these measurements. First, the on/off ratio of graphene transistors with ion-gel gating was greater than 10 between gate voltages of -2 and 2 V . In particular, the on/off ratio of the $[\text{EMIM}]^+\text{NTf}_2^-$ device was more than 100. This is the highest ratio achieved in a graphene transistor to the best of our knowledge. The reason for this is not yet totally understood and needs to be investigated since securing a high on/off ratio for graphene transistors is important in the development of graphene-based high-performance CMOS-like electronic devices. Second, the operational voltage range that did not produce a gate leakage current increased as the molecular weight of the ionic liquid increased. At gate voltages (V_{gs}) over the EW of the ionic liquid, the drain current (I_{ds}) decreased through gate leakage, as shown in Figure 2b. This seemed to be correlated with the EW of the ionic liquid used in the measurement, in particular the anodic limit, as listed in Table 1. Third, the Dirac point voltage of the graphene transistor depended sensitively on the type of ionic liquid.

To examine the variation of the Dirac point voltage with the anion for the imidazolium-based ionic liquids ($[\text{EMIM}]^+$ series), the Dirac point voltage of the

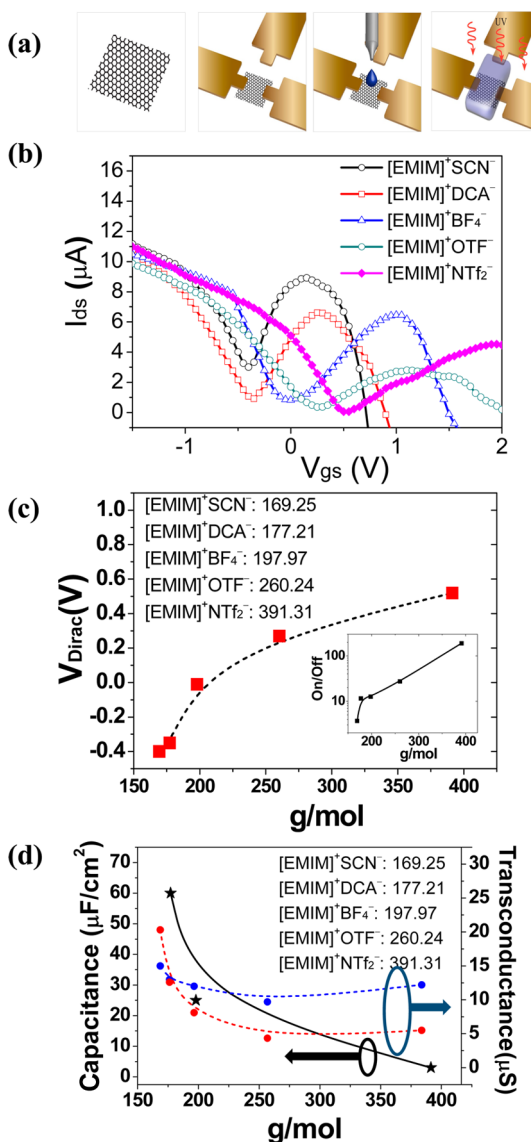
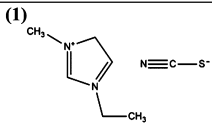
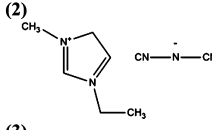
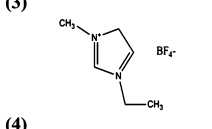
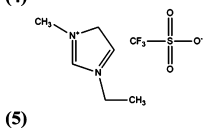
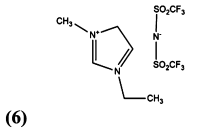
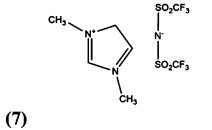
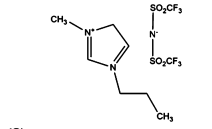
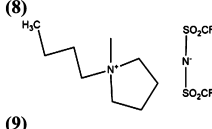
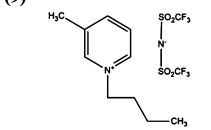


Figure 2. (a) Ion-gel dielectric formation process. (b) Transfer curves (measured at $V_{ds} = 1 \text{ mV}$) for graphene transistors incorporating ion-gel dielectrics with EMIM as the cation and SCN^- , DCA^- , BF_4^- , OTf^- , or NTf_2^- as the anion. (c) Position of the Dirac point voltage (V_{Dirac}) of the ion-gel-gated graphene transistor as a function of the molecular weight of the $[\text{EMIM}]^+$ -bearing ionic liquid. The inset shows the on/off ratios of the devices. (d) Transconductances of electrons (red) and holes (blue) and capacitances taken from the literature (black) as functions of molecular weight for the $[\text{EMIM}]^+$ -based ionic liquids.

ion-gel-gated graphene transistor was plotted as a function of the molecular weight of the ionic liquid; these data are shown in Figure 2c. The inset shows the associated on/off ratios of the devices. Interestingly, the Dirac point voltage shifted to higher voltages, starting from a negative value, as higher-molecular-weight ionic liquids were used. Also, the on/off ratio increased dramatically, up to approximately 200. Finding methods or mechanisms to obtain large on/off ratios of more than one order in FETs using graphene as a channel material must be an essential issue to

TABLE 1. Molecular Structures, Molecular Weights, and Electrochemical Operating Windows of the Ionic Liquids

Molecular Structure	Name of Ionic Liquid	Molecular Weight (g/mol)	Electrochemical Window (V)
(1) 	1-Ethyl-3-methylimidazolium thiocyanate ([EMIM] ⁺ SCN ⁻)	169.25	2.6 (-1.8~0.8) ^a
(2) 	1-Ethyl-3-methylimidazolium dicyanamide ([EMIM] ⁺ DCA ⁻)	177.21	3.0 (-1.6~1.4) ^a
(3) 	1-Ethyl-3-methylimidazolium tetrafluoroborate ([EMIM] ⁺ BF ₄ ⁻)	197.97	4.3 (-2.1~2.2) ^a
(4) 	1-Ethyl-3-methylimidazolium trifluoromethanesulfonate ([EMIM] ⁺ OTF ⁻)	260.24	4.1 (-2.2~1.9) ^a
(5) 	1-Ethyl-3-methylimidazolium bis(trifluoromethanesulfonyl)imide ([EMIM] ⁺ NTf ₂ ⁻)	391.31	4.78 (-2.24~2.54) ^a
(6) 	1-Methyl-3-methylimidazolium bis(trifluoromethanesulfonyl)imide ([DMIM] ⁺ NTf ₂ ⁻)	377.29	N/A
(7) 	1-Propyl-3-methylimidazolium bis(trifluoromethanesulfonyl)imide ([PMIM] ⁺ NTf ₂ ⁻)	405.34	N/A
(8) 	1-Butyl-1-methylpyrrolidinium bis(trifluoromethanesulfonyl)imide ([BMPyr] ⁺ NTf ₂ ⁻)	422.41	6.0 (-3.0~3.0) ^a
(9) 	1-Butyl-3-methylpyridinium bis(trifluoromethanesulfonyl)imide ([BMPy] ⁺ NTf ₂ ⁻)	430.34	N/A

^a From Zhang *et al.*²⁸

optimize and/or maximize the performance of graphene-based electronic devices. Probably, our observation of a large on/off ratio (>100) incorporating [EMIM]⁺NTf₂⁻ provides a better chance to move one step closer in this regard. However, we were not able to find the mechanism for the large on/off ratio at this point. Absolutely, this issue needs to be clarified in the future for the development of graphene-based electronic devices. In Figure 2d, the transconductances ($g_m = \Delta I_{out}/\Delta V_{in} = \Delta I_{ds}/\Delta V_{gs}$) of electrons and holes are plotted as functions of the molecular weight of the ionic liquid alongside the capacitance. The capacitances of the ionic liquids (taken from the literature) decreased with increasing molecular weight.²⁹

Specifically, the values were 60, 25, and 3 $\mu\text{F}/\text{cm}^2$ at 10 Hz for [EMIM]⁺DCA⁻, [EMIM]⁺BF₄⁻, and [EMIM]⁺NTf₂⁻, respectively. For consistency, we took these values from the same reference because they varied significantly depending on the capacitance measurement configuration/method or the sample preparation method.^{18,22,24,29–31} Similar to the trend in the dependence of the capacitance on the molecular weight, the transconductances of electrons and holes generally decreased with increasing molecular weight of the ionic liquid in the [EMIM]⁺ series. As a consequence, the electron transconductance of the ion-gel-gated transistor appears to be proportional to the capacitance. However, the hole transconductance is relatively

less dependent on the capacitance, as shown in Figure 2d. The field-effect mobility of an ion-gel-gated graphene transistor can be calculated in the linear regime of the transfer characteristic using eq 1. From the I_{ds} versus V_g curve in Figure 2b, the hole (electron) mobilities were found to be 54 (52.5), 120 (81), and 1017 (458) $\text{cm}^2 \text{V}^{-1} \text{s}^{-1}$ for devices gated with $[\text{EMIM}]^+\text{DCA}^-$, $[\text{EMIM}]^+\text{BF}_4^-$, and $[\text{EMIM}]^+\text{NTf}_2^-$, respectively. This behavior is consistent with a previous report in which the field-effect mobility of rubrene single-crystal transistors was found to be inversely proportional to the capacitance of the ionic liquid gate dielectric.²⁹

Next, the anion in the ionic liquid was fixed as NTf_2^- , and the total molecular weight was systematically modulated by the use of various cations (*i.e.*, the “ NTf_2^- series”). First, the molecular weight of the cation was adjusted by changing the length of the alkyl chain linked to the imidazolium core (*i.e.*, $[\text{DMIM}]^+$, $[\text{EMIM}]^+$, and $[\text{PMIM}]^+$; see Table 1). In addition to varying the length of the aliphatic alkyl chain attached to the cationic imidazolium core, we also investigated the effect of introducing aromatic hydrocarbon rings by replacing the imidazolium by pyrrolidinium and pyridinium with a longer alkyl chain (*i.e.*, butyl) along with a methyl group (see Table 1). The transfer curves measured at $V_{ds} = 1$ mV for graphene transistors incorporating ion-gel dielectrics using ionic liquids from the NTf_2^- series (*cf.* entries 6–9 in Table 1) are shown in Figure 3a. The Dirac point voltages and on/off ratios of the devices with NTf_2^- -based ion-gel dielectrics are plotted as functions of the molecular weight of the ionic liquid in Figure 3b.

The Dirac point voltage of the graphene transistors apparently increased monotonously with the molecular weight of the ionic liquid. The on/off ratios were approximately 10, except for the $[\text{EMIM}]^+\text{NTf}_2^-$ device, whose operation was similar to those of the $[\text{EMIM}]^+$ series devices. The operation of the graphene transistor was stable without gate leakage during scans between gate voltages of -2 and 2 V. The low operational voltage originated from the EW of the ionic liquid (see Table 1). Figure 3c demonstrates that the transconductances of the graphene transistors with NTf_2^- -series ion-gel dielectrics were not dramatically altered compared to those of the $[\text{EMIM}]^+$ -series devices shown in Figure 2c. This might be because variation in the capacitance among the ionic liquids of the NTf_2^- series is small compared with that of the $[\text{EMIM}]^+$ series materials. A detailed discussion of the modulation of the Dirac point voltage as a function of molecular weight is provided below in the presentation of the MD simulations. From the I_{ds} versus V_{gs} curve in Figure 3a, the electron (hole) mobilities were found to be 458 (1017) and 290 (510) $\text{cm}^2 \text{V}^{-1} \text{s}^{-1}$ in devices gated with $[\text{EMIM}]^+\text{NTf}_2^-$ and $[\text{BMPy}]^+\text{NTf}_2^-$, respectively.

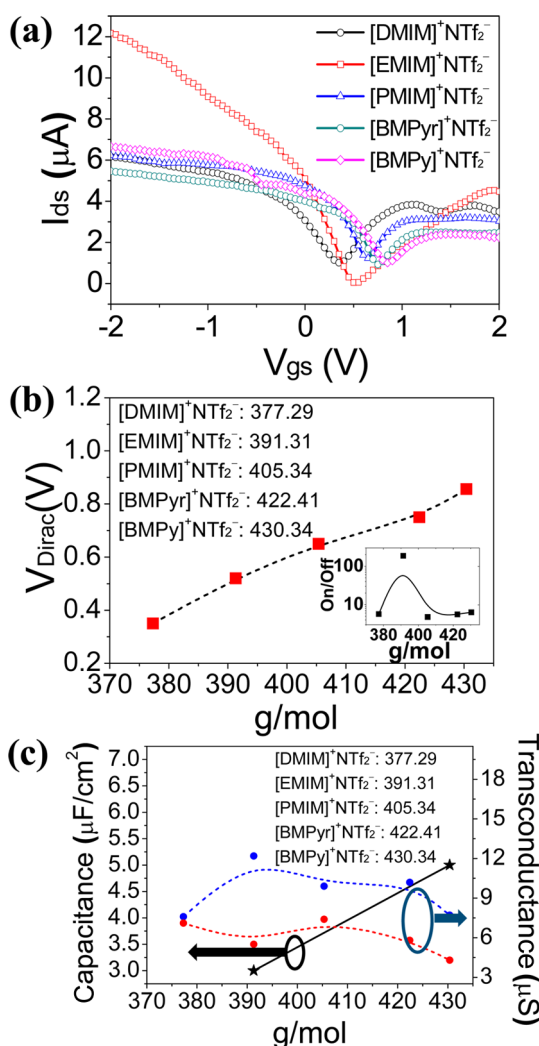


Figure 3. (a) Transfer curves measured at $V_{ds} = 1$ mV for the graphene transistors with NTf_2^- -series ion-gel dielectrics (*i.e.*, $[\text{DMIM}]^+$, $[\text{EMIM}]^+$, $[\text{PMIM}]^+$, $[\text{BMPyr}]^+$, or $[\text{BMPy}]^+$ as the cation). (b) Position of the Dirac point voltage of the transistor as a function of the molecular weight of the ionic liquid in the NTf_2^- series. The inset shows the on/off ratios of the devices. (c) Transconductances of electrons (red) and holes (blue) and capacitances taken from the literature (black) as functions of the ionic liquid molecular weight for the NTf_2^- -series ionic liquids.

Finally, to make use of our findings on the systematic change in the Dirac point voltage of graphene transistors with ionic-liquid gate dielectrics, two different types of ionic liquids whose cations have different molecular features were selected to demonstrate inverters that can be operated at a low supply voltage (V_{DD}). The left side of Figure 4a shows a microscope image of how the inverter was integrated with graphene transistors incorporating $[\text{DMIM}]^+\text{NTf}_2^-$ (left) or $[\text{BMPy}]^+\text{NTf}_2^-$ (right). The graphene transistors for the inverter were of the same materials and at the same scale. The right side of Figure 4a shows a schematic diagram of the graphene transistor covered with ion gel. The side-gate configuration was used in our case. The width of the side gate and its separation from the

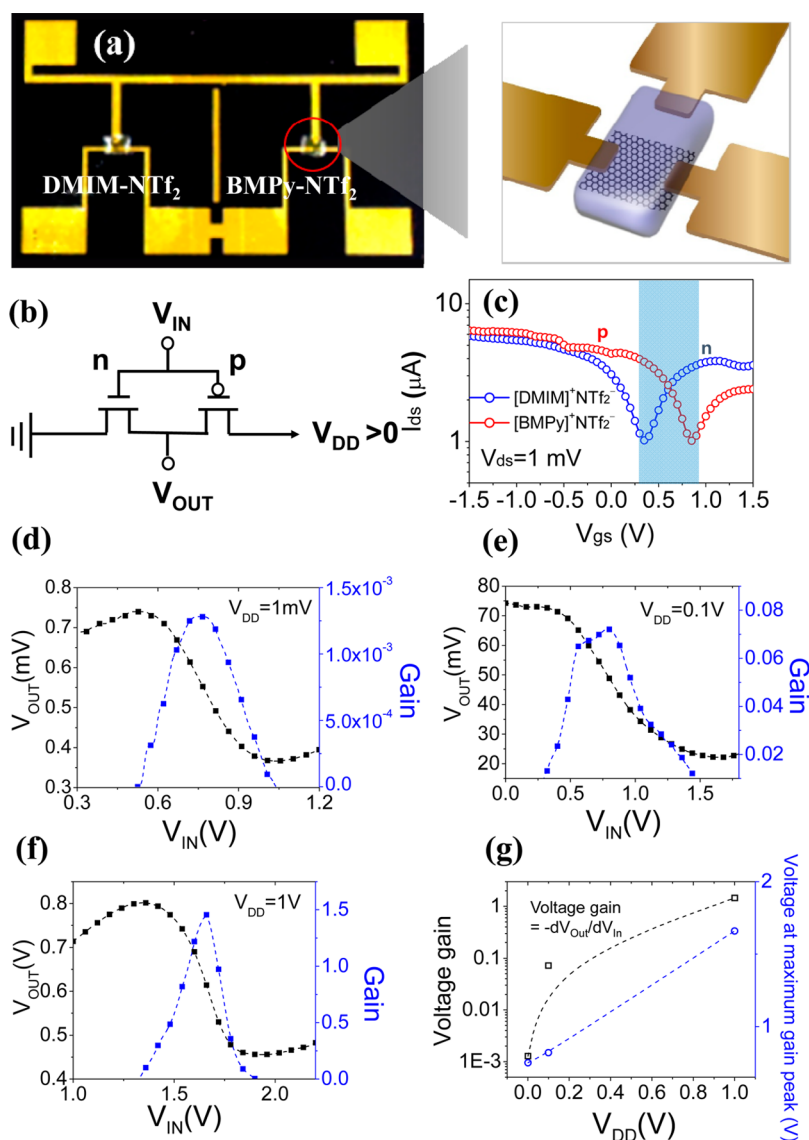


Figure 4. (a) Optical and schematic images of a graphene-based inverter made with ion gels. (b) Inverter circuit diagram. (c) Transfer curves of graphene transistors incorporating [DMIM]⁺NTf₂⁻ and [BMPy]⁺NTf₂⁻ as the gate dielectric. (d–f) Characteristic curves of inverters and their gains obtained at $V_{DD} = 1$ mV, 0.1 V, and 1.0 V, respectively. (g) Position of the maximum peak of the inverter and its gain as functions of V_{DD} .

graphene channel edge were 200 and 220 μm , respectively. [DMIM]⁺NTf₂⁻ and [BMPy]⁺NTf₂⁻-based ionic liquid mixtures were nozzle-printed carefully onto the preintegrated graphene-based inverter backbone formed on the Si/SiO₂ substrate and then hardened by UV cross-linking. Figure 4b shows the idealized inverter circuit diagram for our real device. In the side-gate configuration, each transistor was operated with a different Dirac point position, as shown in Figure 4c. The difference in the Dirac point voltages (ΔV_{Dirac}) was ~ 0.5 V. In the input voltage range of 0.2 to 0.7 V, indicated by the blue shaded area in Figure 4c, the [DMIM]⁺NTf₂⁻ side acted as an n-type transistor and the [BMPy]⁺NTf₂⁻ side as a p-type transistor. Surprisingly, our inverter was fully operational even at a very low supply voltage ($V_{DD} = 1$ mV) with a gain of $\sim 1.4 \times 10^{-3}$, as shown in Figure 4d. We note that the

low gain ($= -V_{\text{out}}/V_{\text{in}}$) was due to the very low value of V_{DD} compared with V_{in} . This low operational voltage (V_{DD}) for the inverter is associated with the unique operational principles of our inverter compared with other types of inverters. For example, in previous studies^{19,22} the graphene-based inverter was demonstrated using only one type of ionic liquid ([EMIM]⁺NTf₂⁻) by integrating two identical graphene transistors. In this type of inverter, one of the Dirac point voltages of the graphene transistors is significantly shifted when the applied drain voltage is sufficiently high (comparable to the gate voltage).^{19,22} Generally, in ambipolar transistors, a point of minimum current is reached when the electron/hole current injected from the source/drain is balanced; this is equivalent to holding the Dirac point voltage at zero gate voltage and applying an equal and opposite

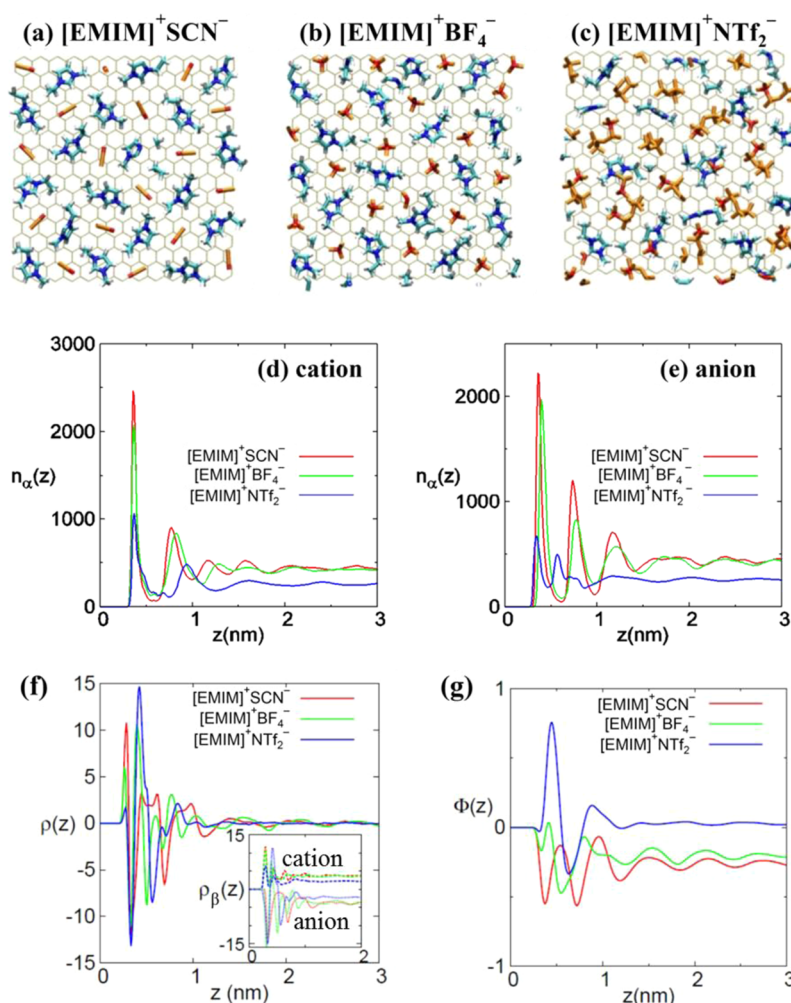


Figure 5. (a–c) Snapshots of the first ion layers in $[\text{EMIM}]^+\text{SCN}^-$, $[\text{EMIM}]^+\text{BF}_4^-$, and $[\text{EMIM}]^+\text{NTf}_2^-$ at 350 K. Bluish and yellowish molecular structures in the snapshots are cations and anions, respectively. (d, e) Number distribution functions $n_\alpha(z)$ (in units of nm^{-3}) as functions of the distance from the graphene surface, z , for (d) N atoms in EMIM^+ cations and (e) carbon, boron, and oxygen atoms in SCN^- , BF_4^- , and NTf_2^- anions, respectively, obtained for $[\text{EMIM}]^+\text{SCN}^-$, $[\text{EMIM}]^+\text{BF}_4^-$, and $[\text{EMIM}]^+\text{NTf}_2^-$ at 350 K. (f) Charge density distribution functions $\rho(z)$ (in units of e/nm^3), decomposed into $\rho_\beta(z)$ for the cations (dotted lines) and anions (solid lines) in the inset, and (g) electric potential $\Phi(z)$ (in units of V) as functions of z obtained for $[\text{EMIM}]^+\text{SCN}^-$, $[\text{EMIM}]^+\text{BF}_4^-$, and $[\text{EMIM}]^+\text{NTf}_2^-$ at 350 K.

voltage ($1/2V_{\text{ds}}$) to the source and drain. The Dirac point voltage, when either the source or drain is grounded, will shift by $1/2\Delta V_{\text{ds}}$ with a change in bias voltage of ΔV_{ds} .²² Previous researchers wisely utilized this phenomenon to integrate CMOS-like devices, inverter and logic gates. In these devices, one transistor acts as n-type and the other as p-type by defining the input voltage to the inverter comprising two identical ambipolar transistors. Despite this innovative approach, the supply voltage (V_{DD}) was relatively high (approximately 1 V or more) because the Dirac point voltage cannot shift with low supply voltage. By contrast, because our work utilized initially existing Dirac point differences originating from two different ionic liquids, it was possible to operate our inverter with significantly reduced V_{DD} (as low as 1 mV). One step forward, our inverter was also tested at higher supply voltages (*i.e.*, $V_{\text{DD}} = 0.1$ and 1.0 V), as shown in Figure 4e,f. As V_{DD} increased, further changes in the Dirac point voltage

differences occurred, and thus, the position of the maximum peak of the inverter shifted by ~ 1 V and the gain increased up to about 1.2 (see Figure 4g). This increased gain is comparable to those obtained in the references.²²

To understand how the behavior of the Dirac point voltage depends on the ionic species in the ionic liquids, we considered the structures of ionic liquids interfacing with a graphene sheet using MD simulations (Figure 5a–c). Detailed information on the simulations is described in the Supporting Information. The number distribution $n_\alpha(z)$ of the center of mass of atom species α , defined by

$$n_\alpha(z) = \int_0^z dz' n_\alpha(z') \quad (2)$$

where $n_\alpha(z_0)$ is the total number of atoms α in the simulation box, was calculated. The results for the average number densities $n_\alpha(z)$ (in units of nm^{-3}) are

displayed in Figure 5d,e. We first considered the results for nitrogen in $[\text{EMIM}]^+$, shown in Figure 5d. In the presence of thiocyanate (SCN^-) or tetrafluoroborate (BF_4^-), the cations formed a strong solvent layer with a thickness of $\Delta z \leq 0.6$ nm from the graphene surface, followed by significant fluctuations with increasing z . This indicates that, on average, ions near the graphene form a layered structure parallel to the surface. This is ascribed to π -stacking interactions between the imidazolium ring and the graphene, as shown in the snapshots in Figure 5a–c, where bluish and yellowish molecular structures in the snapshot are cations and anions, respectively. In $[\text{EMIM}]^+\text{NTf}_2^-$, the number density of the cations decreased because of the large anion size, and the first layer also became weaker and wider ($\Delta z \leq 0.8$ nm). This means that the affinity of the imidazolium-based cation for the graphene grew stronger with smaller anions, such as SCN^- . As for the anions, number distributions of carbon, boron, and oxygen are given in Figure 5e for $[\text{EMIM}]^+\text{SCN}^-$, $[\text{EMIM}]^+\text{BF}_4^-$, and $[\text{EMIM}]^+\text{NTf}_2^-$, respectively. Because of the molecular structure of the linear and small SCN^- anion, the $[\text{EMIM}]^+$ cations tended to be well-aligned with the graphene surface. With bulkier anions, the alignment of the cations with the graphene surface tended to become worse. The first solvent layer of organized anions was much broader with $[\text{EMIM}]^+\text{NTf}_2^-$.

We also examined the electric potential of the ionic liquid–graphene interface. The average charge density distribution $\rho_\beta(z)$ is

$$\rho_\beta(z) = A_0^{-1} \int_0^{x_0} \int_0^{y_0} dx' dy' \rho'_\beta(x', y', z) \quad (3)$$

where $\rho'_\beta(x', y', z)$ is the local charge density arising from the atomic charge distribution of ionic species β ($\beta = +$ for cations and $-$ for anions) and $A_0 = x_0 y_0$. The results for $\rho_\beta(z)$ in three ionic liquids are shown in Figure 5f. Both the cation (dotted lines) and anion (solid lines) charge densities (Figure 5f inset) at $\Delta z \leq 1$ nm showed rapid oscillations in a multiple-layered fashion.

The electric potential $\Phi_\beta(z)$ of ionic species β at various distances z from the graphene surface was calculated by integrating the Poisson equation:

$$\Phi_\beta(z) = -4\pi \int_0^z dz'(z - z')\rho_\beta(z') \quad (4)$$

The total potential $\Phi(z)$ was then obtained as

$$\Phi(z) = \Phi_+(z) + \Phi_-(z) + \Phi_G(z) \quad (5)$$

where $\Phi_G(z)$ is the electric potential introduced by the graphene and ignored for the neutral graphene surface. The total electric potentials for three different ionic liquids are shown in Figure 5g. It should be noted that potentials of zero charge (PZCs) with respect to the bulk region in the center ($\Delta\Phi$) are positive for $[\text{EMIM}]^+\text{SCN}^-$ and $[\text{EMIM}]^+\text{BF}_4^-$ and negative for

$[\text{EMIM}]^+\text{NTf}_2^-$. The interfacial cations paired with SCN^- ions contribute to the positive charge density adjacent to the graphene surface most effectively; this is ascribed to the π -stacking interactions between the imidazolium ring of the cation and the graphene surface in the presence of small anions (see Figure 5a–e). The parallel orientation of cations was significantly disturbed by bulky NTf_2^- , whereas NTf_2^- anions more effectively gave rise to a negative charge density closer to the graphene surface than SCN^- and BF_4^- because of their extended partial atomic charge distributions. As a result, the PZC decreased with increasing anion size from SCN^- to BF_4^- and became negative for $[\text{EMIM}]^+\text{NTf}_2^-$. The rightward shift of the Dirac point voltage to a positive value was caused by the negative charge that accumulated close to the graphene when the anion size increased to that of NTf_2^- . This revealed that $[\text{EMIM}]^+\text{NTf}_2^-$ has a p-doping effect on the graphene, compared with the n-doping induced by $[\text{EMIM}]^+\text{SCN}^-$ or $[\text{EMIM}]^+\text{BF}_4^-$. To gain more insight into the behavior of the Dirac point voltage, we also performed MD simulations to determine the conditions under which $\Delta\Phi = 0$ by changing the charge distribution in the graphene. From the simulations, atomic charges per graphene carbon of $-0.0015e$, $-0.0008e$, and $+0.0002e$ gave $\Delta\Phi(z) = 0$ for $[\text{EMIM}]^+\text{SCN}^-$, $[\text{EMIM}]^+\text{BF}_4^-$, and $[\text{EMIM}]^+\text{NTf}_2^-$, respectively.

Despite the nonpolarizable behavior of the models, these MD results were in good agreement with the experimental results shown in Figure 2. More significant p-doping effects were obtained by enhancing the steric effect of the cation. The same trend was observed in our experiments; the Dirac point voltage shifted to higher values as we increased the length of the alkyl chain of the imidazolium-based cation ($[\text{DMIM}]^+$, $[\text{EMIM}]^+$, and $[\text{PMIM}]^+\text{NTf}_2^-$) or replaced the cation by a pyrrolidinium-based one ($[\text{BMPyr}]^+\text{NTf}_2^-$) that has branched alkyl chains and no π electrons (see Figure 3). These results demonstrate that by utilization of the initial charge-inducing mechanism by ionic liquids on graphene, ionic liquids can be designed or selected.

Finally, graphene, an all-surface material, is extremely sensitive to its surrounding environment, including the supporting substrate, gases, and chemicals.³² Briefly, adsorbed gases on graphene under ambient conditions render the graphene p-type. Meanwhile, the graphene film can be n-type on the SiO_2 surface because of the electron-doping effect from the localized charges in the SiO_2 according to theoretical calculations.³² Considering these, the overall electrical behavior of the FETs observed in our work can also be a result of doping compensation from both the ion gels and the SiO_2 substrates simultaneously. To develop graphene-based soft electronics, it is very important to consider these doping effects and understand the final Dirac point voltage of ion-gel-assisted graphene

transistors, particularly on other types of substrates such as plastics, stretchable polymers, etc. This remains as our future investigation.

CONCLUSIONS

We systematically investigated the effect of different ionic liquids as ion-gel dielectrics on the transfer characteristics of graphene transistors. Ion gels were produced using UV irradiation (for 30 s) of a mixture of a binder, an initiator, and an ionic liquid. By selection of different anions for a fixed cation selection ([EMIM]⁺) or different cations for a fixed anion selection (NTf₂⁻), systematic modulation of the Dirac point voltage of the graphene transistor was achieved. With higher-molecular-weight ionic liquids, the Dirac point voltage of the transistor shifted to higher voltages. The operational voltage of the ion-gel-gated graphene transistor seems to be directly related to the EW of the ionic liquid. Our MD simulations focusing on the interfaces between the graphene and ionic liquids account for the

experimental findings. The imidazolium rings of the cations tend to align parallel to the graphene surface and build up a positive charge density, the extent of which becomes weaker as the anion size increases. As a consequence, [EMIM]⁺NTf₂⁻ effectively generates a negative charge density close to the graphene due to its large anion size and its extended molecular structure. This results in a shift in the Dirac point voltage to a positive value, in good agreement with our experiments. To capitalize on our findings, two different ionic liquids were used to demonstrate inverters that were found to work successfully even at a very low supply voltage of $V_{DD} = 1$ mV with a gain of $\sim 1.4 \times 10^{-3}$. When the supply voltage was increased to 1.0 V, the position of the maximum inverter gain peak shifted to a higher voltage by ~ 1.0 V, and the gain increased to 1.2. These results can be broadly applied in the development of low-power-consumption, flexible/stretchable, CMOS-like graphene-based electronic devices in the future.

EXPERIMENTAL SECTION

Device Fabrication. Graphene was synthesized on a 75 μm thick copper foil by CVD at 985 $^{\circ}\text{C}$ using flowing methane (30 sccm) and hydrogen (100 sccm) for 20 min under vacuum (~ 950 mTorr). The graphene sheet was isolated from the catalyst and transferred onto a Si/SiO₂ (100 nm) substrate by the commonly used “wet” graphene transfer method using PMMA (Aldrich(C4)) as a supporting polymer layer.²⁷ Next, the PMMA was removed by soaking the substrate in acetone/isopropanol. The graphene transistors were fabricated by conventional photolithography methods. Cr (10 nm)/Au (50 nm) were commonly used for source and drain electrodes. The channel length and width were 10 and 40 μm , respectively.

To form ion-gel dielectrics by UV cross-linking, poly(ethylene glycol) diacrylate and 2-hydroxy-2-methylpropiophenone were added to the ionic liquid in a weight ratio of 8:4:88. After the mixture was stirred, it was drop-cast onto the graphene transistor using a nozzle printer (Desktop robot SHOTminiSL/SHOTMASTER 300/500, Musashi) and then immediately treated with UV light (Lichtzen Co., Ltd.) for 30 s to prevent it from flowing significantly before the cross-linking was completed.

Measurement. Raman spectra and maps of the graphene devices were acquired using a Nanobase (XperRam 200) instrument with a 532 nm laser line. All of the electrical data were measured using a Keithley 4200 semiconductor characterization system at room temperature.

Conflict of Interest: The authors declare no competing financial interest.

Supporting Information Available: Simulation models and methods. This material is available free of charge via the Internet at <http://pubs.acs.org>.

Acknowledgment. This CRI work was supported by a National Research Foundation of Korea (NRF) grant funded by the Korean Government (MEST) (NRF-2007-0054845). This work was supported by the Gachon University Research Fund of 2014 (Grant GCU-2014-0123).

REFERENCES AND NOTES

- Liao, L.; Lin, Y. C.; Bao, M. Q.; Cheng, R.; Bai, J. W.; Liu, Y. A.; Qu, Y. Q.; Wang, K. L.; Huang, Y.; Duan, X. F. High-Speed Graphene Transistors with a Self-Aligned Nanowire Gate. *Nature* **2010**, *467*, 305–308.

- Wu, Y. Q.; Lin, Y. M.; Bol, A. A.; Jenkins, K. A.; Xia, F. N.; Farmer, D. B.; Zhu, Y.; Avouris, P. High-Frequency, Scaled Graphene Transistors on Diamond-like Carbon. *Nature* **2011**, *472*, 74–78.
- Lin, Y. M.; Jenkins, K. A.; Valdes-Garcia, A.; Small, J. P.; Farmer, D. B.; Avouris, P. Operation of Graphene Transistors at Gigahertz Frequencies. *Nano Lett.* **2009**, *9*, 422–426.
- Reina, A.; Jia, X. T.; Ho, J.; Nezich, D.; Son, H. B.; Bulovic, V.; Dresselhaus, M. S.; Kong, J. Large Area, Few-Layer Graphene Films on Arbitrary Substrates by Chemical Vapor Deposition. *Nano Lett.* **2009**, *9*, 30–35.
- Berger, C.; Song, Z. M.; Li, T. B.; Li, X. B.; Ogbazghi, A. Y.; Feng, R.; Dai, Z. T.; Marchenkov, A. N.; Conrad, E. H.; First, P. N.; de Heer, W. A. Ultrathin Epitaxial Graphite: 2D Electron Gas Properties and a Route toward Graphene-Based Nanoelectronics. *J. Phys. Chem. B* **2004**, *108*, 19912–19916.
- Novoselov, K. S.; Geim, A. K.; Morozov, S. V.; Jiang, D.; Zhang, Y.; Dubonos, S. V.; Grigorieva, I. V.; Firsov, A. A. Electric Field Effect in Atomically Thin Carbon Films. *Science* **2004**, *306*, 666–669.
- Tung, V. C.; Allen, M. J.; Yang, Y.; Kaner, R. B. High-Throughput Solution Processing of Large-Scale Graphene. *Nat. Nanotechnol.* **2009**, *4*, 25–29.
- Lee, S. K.; Kim, B. J.; Jang, H.; Yoon, S. C.; Lee, C.; Hong, B. H.; Rogers, J. A.; Cho, J. H.; Ahn, J. H. Stretchable Graphene Transistors with Printed Dielectrics and Gate Electrodes. *Nano Lett.* **2011**, *11*, 4642–4646.
- Chae, S. H.; Yu, W. J.; Bae, J. J.; Duong, D. L.; Perello, D.; Jeong, H. Y.; Ta, Q. H.; Ly, T. H.; Vu, Q. A.; Yun, M.; Duan, X.; Lee, H. L. Transferred Wrinkled Al₂O₃ for Highly Stretchable and Transparent Graphene–Carbon Nanotube Transistors. *Nat. Mater.* **2013**, *12*, 403–409.
- Bae, S.; Kim, H.; Lee, Y.; Xu, X. F.; Park, J. S.; Zheng, Y.; Balakrishnan, J.; Lei, T.; Kim, H. R.; Song, Y. I.; Kim, Y.-J.; Kim, K. S.; Özyilmaz, B.; Ahn, J.-H.; Hong, B. H.; Iijima, S.; Balakrishnan, J.; Lei, T. Roll-to-Roll Production of 30-Inch Graphene Films for Transparent Electrodes. *Nat. Nanotechnol.* **2010**, *5*, 574–578.
- Eda, G.; Fanchini, G.; Chhowalla, M. Large-Area Ultrathin Films of Reduced Graphene Oxide as a Transparent and Flexible Electronic Material. *Nat. Nanotechnol.* **2008**, *3*, 270–274.
- Liao, L.; Bai, J. W.; Qu, Y. Q.; Huang, Y.; Duan, X. F. Single-Layer Graphene on Al₂O₃/Si Substrate: Better Contrast and

- Higher Performance of Graphene Transistors. *Nanotechnology* **2010**, *21*, No. 015705.
- Chen, F.; Xia, J. L.; Ferry, D. K.; Tao, N. J. Dielectric Screening Enhanced Performance in Graphene FET. *Nano Lett.* **2009**, *9*, 2571–2574.
 - Li, S. L.; Miyazaki, H.; Lee, M. V.; Liu, C.; Kanda, A.; Tsukagoshi, K. Complementary-like Graphene Logic Gates Controlled by Electrostatic Doping. *Small* **2011**, *7*, 1552–1556.
 - Konar, A.; Fang, T. A.; Jena, D. Effect of High- κ Gate Dielectrics on Charge Transport in Graphene-Based Field Effect Transistors. *Phys. Rev. B* **2010**, *82*, 115452.
 - Hollander, M. J.; LaBella, M.; Hughes, Z. R.; Zhu, M.; Trumbull, K. A.; Cavalero, R.; Snyder, D. W.; Wang, X. J.; Hwang, E.; Datta, S.; Robinson, J. A. Enhanced Transport and Transistor Performance with Oxide Seeded High- κ Gate Dielectrics on Wafer-Scale Epitaxial Graphene. *Nano Lett.* **2011**, *11*, 3601–3607.
 - Cho, J. H.; Lee, J.; Xia, Y.; Kim, B.; He, Y. Y.; Renn, M. J.; Lodge, T. P.; Frisbie, C. D. Printable Ion-Gel Gate Dielectrics for Low-Voltage Polymer Thin-Film Transistors on Plastic. *Nat. Mater.* **2008**, *7*, 900–906.
 - Lee, J.; Kaake, L. G.; Cho, J. H.; Zhu, X. Y.; Lodge, T. P.; Frisbie, C. D. Ion Gel-Gated Polymer Thin-Film Transistors: Operating Mechanism and Characterization of Gate Dielectric Capacitance, Switching Speed, and Stability. *J. Phys. Chem. C* **2009**, *113*, 8972–8981.
 - Ha, M. J.; Xia, Y.; Green, A. A.; Zhang, W.; Renn, M. J.; Kim, C. H.; Hersam, M. C.; Frisbie, C. D. Printed, Sub-3V Digital Circuits on Plastic from Aqueous Carbon Nanotube Inks. *ACS Nano* **2010**, *4*, 4388–4395.
 - Kang, Y. J.; Chun, S. J.; Lee, S. S.; Kim, B. Y.; Kim, J. H.; Chung, H.; Lee, S. Y.; Kim, W. All-Solid-State Flexible Supercapacitors Fabricated with Bacterial Nanocellulose Papers, Carbon Nanotubes, and Triblock-Copolymer Ion Gels. *ACS Nano* **2012**, *6*, 6400–6406.
 - Kang, Y. J.; Chung, H.; Kim, W. 1.8-V Flexible Supercapacitors with Asymmetric Configuration Based on Manganese Oxide, Carbon Nanotubes, and a Gel Electrolyte. *Synth. Met.* **2013**, *166*, 40–44.
 - Kim, B. J.; Lee, S. K.; Kang, M. S.; Ahn, J. H.; Cho, J. H. Coplanar-Gate Transparent Graphene Transistors and Inverters on Plastic. *ACS Nano* **2012**, *6*, 8646–8651.
 - Chen, F.; Qing, Q.; Xia, J. L.; Li, J. H.; Tao, N. J. Electrochemical Gate-Controlled Charge Transport in Graphene in Ionic Liquid and Aqueous Solution. *J. Am. Chem. Soc.* **2009**, *131*, 9908–9909.
 - Lee, S. W.; Lee, H. J.; Choi, J. H.; Koh, W. G.; Myoung, J. M.; Hur, J. H.; Park, J. J.; Cho, J. H.; Jeong, U. Periodic Array of Polyelectrolyte-Gated Organic Transistors from Electrospun Poly(3-hexylthiophene) Nanofibers. *Nano Lett.* **2010**, *10*, 347–351.
 - Lee, S. W.; Kim, B. S.; Park, J. J.; Hur, J. H.; Kim, J. M.; Sekitani, T.; Someya, T.; Jeong, U. High Performance Foldable Polymer Thin Film Transistors with a Side Gate Architecture. *J. Mater. Chem.* **2011**, *21*, 18804–18809.
 - Lee, S. K.; Kabir, S. M. H.; Sharma, B. K.; Kim, B. J.; Cho, J. H.; Ahn, J. H. Photo-Patternable Ion Gel-Gated Graphene Transistors and Inverters on Plastic. *Nanotechnology* **2014**, *25*, No. 014002.
 - Kim, U. J.; Hur, J.; Cheon, S.; Chung, D. Y.; Son, H.; Park, Y.; Roh, Y. G.; Kim, J.; Lee, J.; Kim, S. W.; Im, K.; Park, N.; Kim, J.; Hwang, S.; Park, W.; Lee, C.-W. Enhancement of Integrity of Graphene Transferred by Interface Energy Modulation. *Carbon* **2013**, *65*, 165–174.
 - Zhang, S. J.; Sun, N.; He, X. Z.; Lu, X. M.; Zhang, X. P. Physical Properties of Ionic Liquids: Database and Evaluation. *J. Phys. Chem. Ref. Data* **2006**, *35*, 1475–1517.
 - Ono, S.; Miwa, K.; Seki, S.; Takeya, J. A Comparative Study of Organic Single-Crystal Transistors Gated with Various Ionic-Liquid Electrolytes. *Appl. Phys. Lett.* **2009**, *94*, No. 063301.
 - Liu, J. K.; Qian, Q. K.; Zou, Y.; Li, G. H.; Jin, Y. H.; Jiang, K. L.; Fan, S. S.; Li, Q. Q. Enhanced Performance of Graphene Transistor with Ion-Gel Top Gate. *Carbon* **2014**, *68*, 480–486.
 - Kim, B. J.; Jang, H.; Lee, S. K.; Hong, B. H.; Ahn, J. H.; Cho, J. H. High-Performance Flexible Graphene Field Effect Transistors with Ion Gel Gate Dielectrics. *Nano Lett.* **2010**, *10*, 3464–3466.
 - Romero, H. E.; Shen, N.; Joshi, P.; Gurierrez, H. R.; Tadigadapa, S. A.; Sofo, J. O.; Eklund, P. C. N-Type Behavior of Graphene Supported on Si/SiO₂ Substrates. *ACS Nano* **2008**, *2*, 2037–2044.